Available at www.sciencedirect.com

ScienceDirect

journal homepage: www.elsevier.com/locate/he

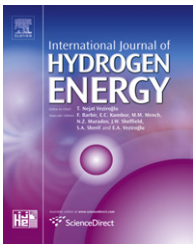

Thermal design of a solar hydrogen plant with a copper–chlorine cycle and molten salt energy storage

Z. Wang, G.F. Naterer, K.S. Gabriel, E. Secnik, R. Gravelsins, V. Daggupati*

Faculty of Engineering and Applied Science, University of Ontario Institute of Technology, 2000 Simcoe St N, Oshawa, Ontario, Canada

ARTICLE INFO

Article history:
Received 20 August 2010
Received in revised form
26 November 2010
Accepted 2 December 2010
Available online 14 January 2011

Keywords:
Solar hydrogen production
Copper–chlorine cycle
Molten salt

ABSTRACT

In this paper, the operating temperature ranges of various solar thermal energy technologies are analyzed, with respect to their compatibility with solar hydrogen production via thermochemical cycles. It is found that the maximum temperature of 530 °C required by the oxygen production step in the Cu–Cl cycle can be supplied by current solar thermal technologies. The heat requirements are examined for the Cu–Cl cycle and it is found that the heat source must be sufficiently high and above the maximum temperature requirement of the Cu–Cl cycle, in order to match the heat requirements of the cycle. The quantity of molten salt and solar plant dimensions for capturing and storing solar heat for an industrial hydrogen production scale are also estimated for 24 h operation per day. The flow characteristics and heat losses of molten salt transport in pipelines are studied while considering the influences of pipeline diameter, heat load and weather conditions. The heat loss from a solar salt storage tank is also calculated based on various tank diameters and heights. The intermediate product of molten salt produced in the oxygen production step gives the Cu–Cl cycle a significant advantage of linkage with current high temperature solar thermal technologies. This allows flexibility for integration of the Cu–Cl cycle and solar thermal plant. Using a thermal network analysis of the Cu–Cl cycle, the layout options for the integration of a Cu–Cl cycle with various solar thermal technologies are presented and discussed in this paper.

1. Introduction

Targets to meet the growing demand for energy, and at the same time reduce greenhouse gas emissions, have stimulated the growing interest in using hydrogen as a clean fuel. Hydrogen demand in refineries and fertilizer industries is also vigorously rising due to the increasing demand of heavy oil upgrading and food production. The increasing demand for hydrogen has promoted active research on the technologies of producing hydrogen. The future hydrogen supply must be based on clean, secure, and environmentally acceptable production methods. Currently, over 95% of hydrogen is produced via fossil fuels such as steam methane reforming (SMR) at oil refineries [1]. Thermal water splitting technology, with no use of any hydrocarbon, has been viewed as a promising clean alternative to hydrogen production [2–5]. In this technology, thermal energy is the major energy input, either for direct or indirect splitting of water. In the direct splitting method with no auxiliary chemicals or catalysts, the hydrogen can be produced directly once the temperature reaches about 2000 °C [12,32,37]. To lower the temperature, engineers and scientists have developed numerous indirect water splitting methods such as “thermochemical water splitting”, in which water firstly reacts with some other chemicals to form intermediate compounds, then hydrogen and oxygen dissociate from the compounds [10].

The thermal energy sources for thermal water splitting could be nuclear, solar or other sources such as industrial

* *Corresponding author.*
E-mail address: greg.naterer@uoit.ca (G.F. Naterer).
0360-3199/$ – see front matter
doi:10.1016/j.ijhydene.2010.12.003

waste heat. Due to issues such as spent fuel disposal [7–9], numerous studies have been conducted to reduce the environmental impact of long-term waste disposal from nuclear plants. In addition, solar energy is also an attractive option for the thermal energy supply for thermochemical hydrogen production [2–4].

During the past several decades, many thermochemical cycles have been developed for the production of hydrogen from water. It has been shown that some cycles have the potential to deliver overall system efficiencies in excess of 40% [2,6,13]. Among these cycles, the sulfur–iodine (S–I), hybrid sulfur and copper–chlorine (Cu–Cl) cycles are under active investigation and scale-up [2,5,6,11]. Since thermochemical cycles require thermal energy to chemically decompose water to form intermediate compounds, and then dissociate the compounds to give hydrogen and oxygen, the temperature and heat transfer rate must be supplied by a high temperature heat source. It is preferable that the chemical reactors used in thermochemical cycles can be easily integrated with existing or near-future solar thermal concentration systems. This paper will firstly compare the temperatures of solar thermal technologies and typical thermochemical cycles, then establish the heat requirements and structure of the Cu–Cl cycle. Based on industrial hydrogen production scales comparable with SMR, the flow characteristics and heat losses in the pipeline are examined based on various heat loads, pipeline diameters and weather conditions. The molten salt flow rate, solar plant size and heat losses through a storage tank will also be studied to provide a quantitative approximation. Layout options for a solar Cu–Cl thermochemical hydrogen production plant will be presented and discussed. The unique advantages of the Cu–Cl cycle to couple with solar thermal equipment are discussed as well.

2. Matching heat flows of solar concentrator and thermochemical cycles

2.1. *Temperature levels of solar thermal technologies*

Currently, there are five major solar thermal concentrating technologies in various stages of development and commercialization. These technologies are: heliostat solar thermal tower, parabolic dish reflector, parabolic trough reflector, linear reflective Fresnel lens, and refractive Fresnel lens. The heliostat solar thermal tower uses arrays of solar tracking heliostat mirrors to reflect incident rays to a tall tower where a water or air tank can be installed to absorb the reflected solar rays for direct steam generation and gas turbine. The tank can also be a molten salt receiver that is used to produce steam or store the solar thermal energy, for use at night, or cloudy and rainy days [29,39]. In the parabolic reflector technology, a two-axis tracking parabolic dish reflector focuses the solar radiation onto a Stirling cycle system to directly generate electricity, with no need of steam generation. The refractive Fresnel lens technology is similar to the parabolic dish system, but it uses downward concentrated refractive solar radiation rather than upward reflection. Both parabolic reflector and refractive Fresnel lens technologies can reach a very high temperature of 2000 °C, which is much higher than a heliostat solar tower. However, the heliostat solar tower can reach a larger generation scale in a single unit that concentrates the reflections from thousands of mirrors [14]. By comparison, a Stirling engine is often combined with an individual parabolic dish or refractive Fresnel lens for power generation [19,25]. Therefore, it is more straightforward for a thermochemical cycle to couple with a single heliostat solar tower than many parabolic dishes.

A parabolic trough is generally constructed as a long parabolic reflective mirror with a receiving tube at the focal line. The linear reflective Fresnel concentrating technology is similar to the parabolic trough system, but it uses a Fresnel lens to concentrate the reflected solar rays to the receiving tube at the focal line. The tube is filled with heat transfer oils or low melting point salts to absorb the reflected solar radiation. The heated oils or salts are pumped to a steam generator and the generated steam is used to drive a turbine. Since the trough or reflective lens is usually aligned on a north-south axis to track the sun, the solar radiation parallel with the axis cannot be concentrated. Moreover, the surface area of each trough or Fresnel lens is limited by its size. The maximum temperature of the heat transfer fluid in current solar trough or reflective lens technology is 450 °C [28,29,39], which is lower than that of a heliostat solar tower that can concentrate the solar rays reflected by thousands of heliostat mirrors. From the perspective of the temperature requirement, a heliostat solar tower can provide higher temperatures than a parabolic reflective trough or Fresnel lens for the integration with a thermochemical hydrogen production cycle. The focus of the following discussion will be on the heliostat solar thermal tower technology.

A pilot-scale solar thermal tower (Sierra Suntower) operating in California uses a cavity receiver to directly generate steam at 440 °C. Its gross electrical power output is 5 MW in a Rankine cycle [15,16]. Two commercially operating solar towers (PS10 and PS20 solar towers) in Seville, Spain, give a higher power output of 11 MW and 20 MW, but the steam has a considerably lower temperature of 250–255 °C [19,20].

The first industrial scale solar thermal tower (Solar 2 Tower) uses molten salt as its energy capturing fluid. It was developed by the US Department of Energy and operated at 565 °C from 1998 to 1999 in Barstow, California [14,17,18]. Steam was generated from a molten salt steam generator and the power output was 10 MW. This is equivalent to the operating PS10 Solar Tower of Spain. An outstanding advantage of using molten salt as the medium is that the solar heat can be stored for tens of hours for use at night, or weather when sunlight is not available.

The salt-free tower operating in Germany (Jülich Solar Tower) is the world's first solar thermal power plant that uses air as the working fluid for pilot-scale heat capturing [21,22]. The air temperature can reach 1000 °C and a gas turbine is adopted for power generation with the output of 1.5 MW. The disadvantage of this technology is the difficulty to store solar heat for night use. However, the gas turbine can also be driven by fossil or biomass fuels so that the tower can supply fuel power at times of no solar energy [23].

France operated a small pilot-scale solar thermal tower (THEMIS Solar Tower) that gave 2 MW power output between 1983 and 1986 [19,24,25]. The molten salt temperature was

450 °C and the steam generated from the molten salt was 430 °C.

Spain is constructing a molten salt solar tower (Solar Tres) that will have a power output of 17 MW [26,27]. The tower is based on the technology of the Solar 2 Tower of California, US [17,18]. The temperature of the molten salt for steam generation is 565 °C.

Two heliostat solar thermal towers (LPT 550 and LPT 650 towers) have been announced for construction in California [28]. The towers will use a water receiver to absorb the reflected solar radiation to directly generate superheated steam at 550 °C and 650 °C. Each tower has a nominal power output of 100 MW.

China has announced a project to build a heliostat solar thermal tower that will have a power output of 1 MW for research and development purposes [30]. The working fluid for the solar receiver could be water, thermal oil or molten salt. The steam temperature is designed for 400 °C.

2.2. *Temperature levels of thermochemical hydrogen production cycles*

Fig. 1 gives the maximum temperatures required by some typical thermochemical cycles. It summarizes the temperature levels of various solar technologies that are currently operational, under construction and announced.

A thermochemical hydrogen production cycle generally consists of several steps, either chemical reactions or physical processes. Some steps require heat at high temperatures, and the maximum temperature needed by a step is the threshold that limits the availability of solar thermal energy.

Fig. 1 shows that the Cu–Cl cycle has the minimum temperature threshold for integration with solar technologies, especially with the heliostat solar tower that is currently operational and can reach a large energy scale in a single solar radiation receiver. To examine the temperature matching in detail, the steps of a typical Cu–Cl cycle are listed below as follows [2,5,6,11].

Step 1: Hydrogen production step (electrolysis)

$$2CuCl(aq) + 2HCl(aq) = 2CuCl_2(aq) + H_2(g), \text{ in aqueous solution of HCl, } 80–100\ ^\circ C \quad (1)$$

Step 2: Drying step (endothermic)

$$CuCl_2(aq) + n_f H_2O(l) = CuCl_2 \cdot n_h H_2O(s) + (n_f - n_h)H_2O \quad n_f > 7.5,\ n_h = 0–4, \text{ at } 30–80\ ^\circ C \text{ (crystallization) or } 60–100\ ^\circ C \text{ (spray drying)} \quad (2)$$

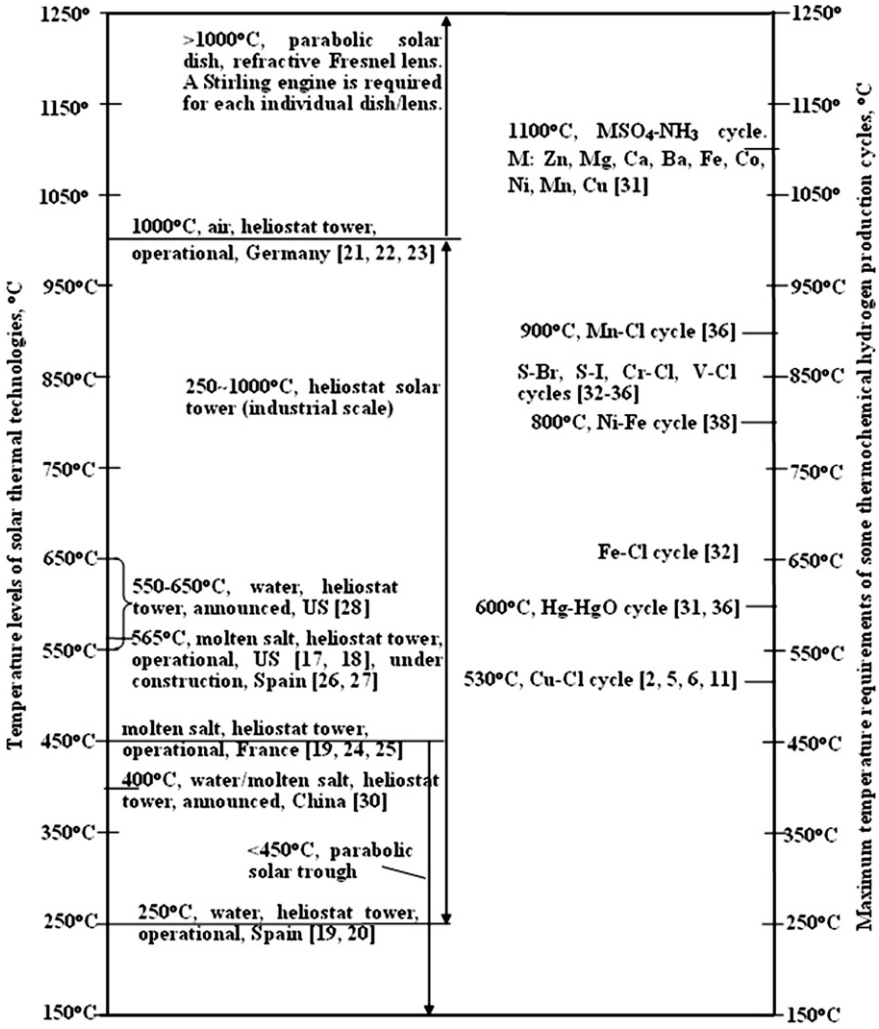

Fig. 1 – Temperature levels of solar thermal technologies and thermochemical hydrogen production cycles.

Table 1 – Distribution of heat requirements of the Cu–Cl cycle.

Step[d]	Heat grade, °C	Heat input if no heat is internally recovered,[b] kJ/mol H_2	Heat output,[a] kJ/mol H_2	Net heat input at 50% heat recovery,[b] kJ/mol H_2	Compared with the total net heat input at 50% heat recovery,[b,c] %
1	<100 °C	0 (Electricity: 52.3 kJ/mol H_2)	0	0	0%
2	<200 °C	122.2	0	122.2	26.9%
3	≥375 °C	227.9	0	181.8[c]	40.1%
4	≥530 °C	149.4	92.2	149.4	33.0%
Sum[d]		499.5	92.2	453.4 (226.7 MJ/kg H_2)	100%

Ratio of electricity (required by step 1) to total net heat flow (required by steps 2, 3 and 4): 15/100.
a Heat output: the heat released by exothermic processes of the Cu–Cl cycle.
b 50% Heat recovery: 50% of the heat released by exothermic processes of the Cu–Cl cycle is recovered.
c 50% Recovered heat is transferred to step III.
d Each step includes all unlisted auxiliary processes [6,13].

Step 3: Hydrolysis step (endothermic)

$$2CuCl_2 \cdot n_h H_2O(s) + H_2O(g) = CuOCuCl_2(s) + 2HCl(g) + n_h H_2O(g),\ n_h \text{ is 0–4, at 375 °C} \quad (3)$$

Step 4: Oxygen production step (endothermic)

$$CuOCuCl_2(s) = 2CuCl(molten) + 0.5O_2(g), \text{ at 530 °C} \quad (4)$$

It can be found that the temperature requirement for the steam of step 3 is 375 °C, which is 155 °C lower than the temperature required by step 4. This indicates that the steam generated from the solar molten salt can also be directly used for step 3 when the molten salt is supplying heat to step 4. This allows flexibility for thermal integration of the Cu–Cl cycle and a solar thermal plant.

2.3. *Matching the delivered and required heat distributions*

Hydrogen production scale is significantly influenced by the available heat quantity provided by the solar thermal plant. Even if the temperature of solar thermal working fluid can cover the maximum temperature requirement of 530 °C, it may not match the heat distribution required by different temperatures of various steps in the Cu–Cl cycle. Table 1 shows the heat requirements of the Cu–Cl cycle [13]. Different steps occupy a different heat requirement percentage. If the heat source does not match the required temperatures, then one or two steps may not be supplied with sufficient heat, and simultaneously other steps may be supplied with surplus heat. Therefore, the temperature of the heat source should not only cover the maximum temperature requirement of the Cu–Cl cycle, but it should also provide a similar heat requirement distribution.

The distribution of heat source depends on the working fluid temperatures entering and exiting the Cu–Cl cycle. Due to the high heat capacity and low volume and pressure requirements, molten salt is selected as the working fluid for analysis in this paper. To store the thermal energy for use over 24 h, there must be sufficient molten salt stored in the tanks. Due to the design and operation complexity when working with phase change heat exchangers, only sensible heat of solar salt is considered for the heating purpose of producing hydrogen. The energy storage capacity depends on the thermodynamic properties of the salt, the available temperature of the salt, and the size of the storage tank. Table 2 shows the thermochemical properties of the solar salt used at UOIT for the integration of the Cu–Cl cycle and a solar thermal storage tank. Although the properties are not identical to those in existing operational towers, it is anticipated that a reasonable approximation is approached since similar salts are adopted in existing operational solar thermal towers [43,44].

The temperature of molten salt leaving the Cu–Cl cycle should be sufficiently higher than the melting point to offset the heat loss in the molten salt transport through a pipeline between the solar and hydrogen production plants, and also to avoid solidification on the inner wall of the pipeline. In this paper, 300 °C is selected as the temperature of molten solar salt exiting the Cu–Cl cycle, which is about 80 °C higher than the melting point. Later sections of this paper will discuss the details of the temperature selection criteria based on the calculations of the heat loss. Since only sensible heat of molten solar salt is provided to the Cu–Cl cycle, the deliverable heat distribution of molten salt can be estimated by variations of the molten salt temperature drop passing through each step of the Cu–Cl cycle. The matching criterion is that higher grade heat should be met at a higher priority

Table 2 – Thermodynamic properties of Hitec solar salt (60-40 salt) used for solar working fluid.

Composition, wt%	Melting point	Boiling point	Average density (222–540 °C)	Average heat capacity (222–540 °C)	Average viscosity (222–540 °C)	Average thermal conductivity (222–540 °C)
59–61% $NaNO_3$ 39–41% KNO_3	222 °C	704 °C	1794 kg/m^3	2.884 MJ/m^3 K (1.549 kJ/kg K)	2.1 cp	3.635 W/m K

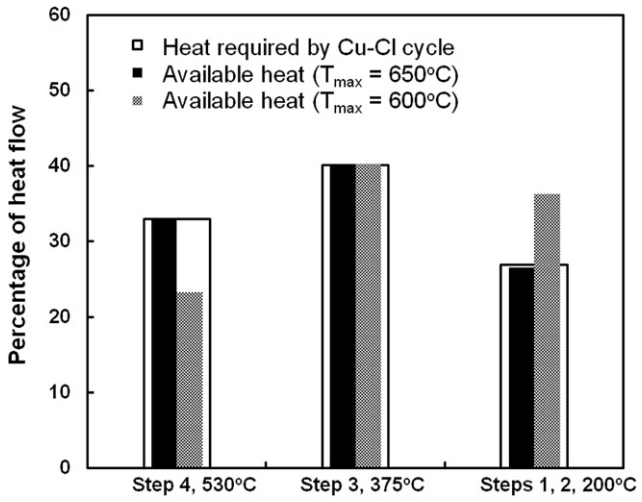

Fig. 2 – Heat distribution of Cu–Cl cycle and solar heat source at various temperatures.

since lower grade heat may be met by the exiting heat of higher grade steps.

Fig. 2 shows the matching extent for various maximum deliverable temperatures of the heat source. It can be found that 600 °C can cover the maximum temperature requirement of 530 °C of step 4 in the Cu–Cl cycle, but it does not have a sufficient heat percentage for step 4 while also a surplus heat flow for steps 1 and 2. To satisfy the heat requirements of step 4, the mass flow rate of molten solar salt must be increased, but this will deliver surplus heat for other steps, and as a result, the temperature exiting the Cu–Cl cycle will increase. This will reduce the overall thermal efficiency of both solar and hydrogen production plants. Increasing the entering temperature is another potential solution to satisfy the requirement. Fig. 2 shows that the deliverable temperature must be increased to higher than 650 °C, so as to match the heat requirements of the Cu–Cl cycle. The temperature drop of the molten salt passing through each step of the Cu–Cl cycle can be readily adjusted to match the heat distribution network when the maximum deliverable temperature of molten salt is higher than 650 °C. Fig. 3 shows the matching of deliverable and required temperatures for each step of the Cu–Cl cycle after considering the heat loss in the pipeline. The heat loss is influenced by the molten salt flow rate among other parameters, which will be discussed in the following section. If the salt exiting the hydrogen plant directly enters the high temperature salt storage tank, then the mixing will reduce the available temperature. Therefore, a low temperature buffer tank to receive the low temperature salt from the hydrogen plant is needed. Then those storage tanks can switch the operation between high and low temperatures to avoid mixing of low and high temperature salts.

2.4. *Heat storage and solar plant dimensions at various hydrogen production scales*

The molten salt quantity and heat load are determined by the hydrogen production scale and storage time of solar thermal energy. Past experiments showed that the capturing efficiency of solar radiation with solar heliostats and lens is about 70% of the solar direct radiation of 1.05 kW/m^2 [18,19]. The heat loss to the environment from the solar thermal fluid can be controlled below 20%, due to the conveying distance and storage time, which will be discussed in later sections of this

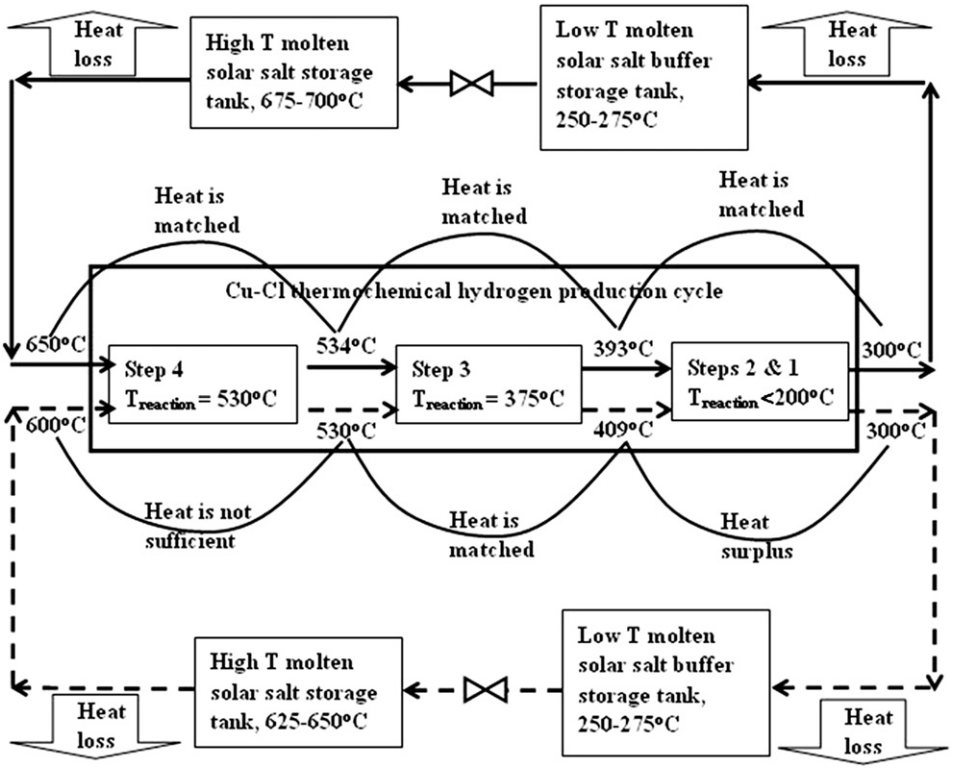

Fig. 3 – Matching the heat distribution of the Cu–Cl cycle by heat source and heat losses.

Table 3 – Heat load, solar salt quantity, mirror and land areas at various hydrogen production scales.

H_2 production scale (t/day)		Heat required[a] (H_2 production: 24 h/day), MW_{th}	Solar salt quantity,[b] t/day	Total mirror area,[c] km^2	Land area,[d] km^2	Diameter of the land area, km	If solar heat is used for power generation only,[e] MWe
Small pilot	1	5.25	627	0.03	0.10	0.37	1.7
Large pilot	10	52.5	6268	0.34	1.04	1.15	17.3
Industrial	100	524.8	62,675	3.43	10.39	3.64	173.2
	200	1049.5	125,351	6.85	20.77	5.14	346.4
	400	2099.1	250,701	13.71	41.54	7.27	692.7

a About 60% of the heat is used to generate the electricity for the electrolysis step of the Cu–Cl cycle. The value 60% is obtained from the ratio of 15–25%, which are the energy percentages and overall efficiency of electrolysis, respectively. Also, assume the total heat loss caused by the storage tank and transport pipeline is 20%.
b The capturing time of solar radiation is averaged at 5 h per day but the stored solar salt is obtained for 24 h of heat supply for hydrogen production each day. The salt uses sensible heat in the temperature range of 250–700 °C for the solar heat storage.
c The calculation of mirror area is based on operational data that 70% of the solar radiation is eventually captured by the molten salt receiver atop the solar tower [18,19]. All of the thermal energy is used for hydrogen production.
d Assume that 1/3 of the land is occupied by the mirrors and the rest of the area is used for passage and other facilities [19,22,25].
e The power generation efficiency from molten salt thermal energy is 33% [18,22,25].

paper. It is assumed that the available run-time for capturing solar radiation is averaged at 5 h per day after considering the weather conditions. Since the hydrogen production cycle is operated 24 h each day, the analysis is based on the assumption that the solar thermal energy is captured in 5 h, but stored and used for 24 h. It is also assumed that the electricity for the electrolysis step of the Cu–Cl cycle is generated from the stored solar thermal energy and the overall electrolysis efficiency is 25%. This represents a multiplication of power generation efficiency (30–35%) and electrolyzer efficiency (80–90%) [18,22,25,46]. From the energy requirement distribution shown in Table 1, the electricity is 15% of the thermal energy, which implies the total captured solar heat should have a factor of (1 + 0.15/0.25) on the basis of the requirement of the thermal steps of the Cu–Cl cycle.

Table 3 lists the molten salt and heat quantities and land areas needed by different hydrogen production scales when coupling a heliostat solar thermal tower with the Cu–Cl thermochemical cycle. The heat quantities listed in Table 1 are used for the calculation on a per mole basis of hydrogen production. Various hydrogen production scales from small pilot to large industrial scales are given and the scale of 100–400 t of hydrogen per day is equivalent to steam methane reforming plants of industrial scales. The power generation capacity utilizing the same amount of solar thermal energy is also given in Table 3, in order to compare it with other power generation plants.

Table 3 suggests a very large land area requirement by a solar plant, either for hydrogen production or only for power generation. For example, the diameter of a solar plant that can produce 400 t hydrogen per day or can generate the power of 693 MW_e is 7 km, which is 4–8 times larger than a nuclear power plant giving the same power output [42]. Table 3 also shows a quarter million tons of molten salt storage for a hydrogen production scale of 400 t per day, which is also a challenge to process such amounts of salt.

To store the large amounts of solar salt indicated in Table 3, a number of storage tanks are needed. Fig. 4 shows the numbers and heights of the tanks. In addition to 700 °C as the maximum storage temperature, other temperatures working as the upper limits are also given in Fig. 4 to show the influence of storage temperature on the tank size. The temperatures higher than 704 °C (boiling point at ambient pressure) are provided only for estimating the temperature effect on molten storage tank height, based on the assumption that the salt remains chemically stable and a liquid state by means of enhancing pressure. Increasing the storage temperature can decrease the tank height for the same amount of heat storage, but the influence is not as significant as the tank diameter. If using only one salt tank to store the solar heat, the tank height can reach hundreds of meters, which is impractical. This is another challenge for the use of large amounts of solar energy. The potential solutions to these challenges include: utilizing salts that can give larger temperature spans between the melting point and upper limit, or using the evaporation heat of salts to store the solar heat if the salt is still chemically stable in the vapor state.

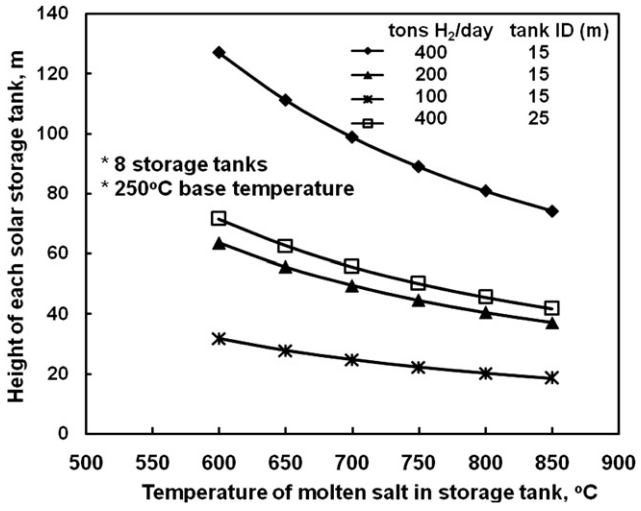

Fig. 4 – Dependence of the height of a solar salt storage tank on hydrogen production scale and the temperature difference between the solar molten salt and Cu–Cl cycle.

2.5. *Characterization of solar heat capturing and storage capacity of molten salt*

To reduce the piping complexity and heat loss, the molten salt storage tanks can be built close to the sunlight concentrating and capturing tower. Then the solar heat capturing and storage capacity can be characterized in a similar way. When using the sensible heat of molten salt to capture and store solar thermal energy, the capturing and storage capacity can be characterized by the molten salt flow rate per unit heat quantity:

$$C_S = \frac{Q_C}{\int_{T_L}^{T_H} C_P dT} \quad (\text{at } Q_C = 1\ MW_{th}) \tag{5}$$

where C_S is the capturing and storage capacity that has units of $kg\,s^{-1}/MW_{th}$, T_L is the minimum temperature to keep the salt at a molten state and at the same time allow a portion of heat loss, which is set at 250 °C as discussed previously. Also, T_H is the upper temperature set at 700 °C that is just below the boiling point, and C_P is the heat capacity of molten salt with a value given in Table 2. Then it can be determined that C_S is $1.4346\ kg\,s^{-1}/MW_{th}$. Based on this value, the calculations of thermal energy storage quantity, heat transport, heat loss and pressure drop in the pipeline can be related to the hydrogen production scale.

3. Heat transport from the solar plant to the thermochemical cycle

3.1. *Molten salt flow characteristics in the transport pipeline*

When utilizing molten salt to transport heat in a pipeline over a distance, the heat loss and transport rate are greatly influenced by the molten salt flow characteristics. The flow parameters such as the flow velocity and pressure loss must be controlled in an acceptable engineering range in the pipeline. The velocity is determined by the molten salt flow rate and pipe diameter. The flow rate can be calculated from C_S and heat load. Fig. 5 shows the dependence of molten salt flow velocity on the heat load. It can be found that the velocity can be controlled below 3 m/s even if the heat load reaches as high as 3000 MW_{th} when the pipeline diameter is larger than 1 m.

Utilizing a smaller diameter pipeline can reduce the construction cost. However, it may generate high pressure losses that require significant pumping power. To estimate the pressure drop, the following equation is adopted [47]:

$$\frac{\Delta P}{L} = f \cdot \frac{1}{D} \cdot \frac{\rho u^2}{2} \tag{6}$$

where $\Delta P/L$ is the pressure drop per unit length (Pa/m), D is the pipeline inside diameter, ρ is the molten salt density and the values are given in Table 2. Also, u is the molten salt velocity and the values are given in Fig. 5, f is the friction factor determined by the Reynolds number and the pipeline inner wall roughness. It is assumed that the pipeline roughness is 45 μm, which is equivalent to the values of commercial steel or wrought iron. Then from the Moody chart, the friction factor can be determined. For example, when hydrogen production scales are 100–200 t per day and the corresponding heat loads of the pipeline must be about 500–1000 MW_{th}, the friction factors are found to be in the range of 0.0122–0.0140. Then from equations (5) and (6), the pressure loss can be calculated by:

$$\frac{\Delta P}{L} = \frac{1}{2}\left(\frac{4}{\pi}\right)^2 \frac{f}{\rho} \cdot C_S^2 \cdot D^{-5} \cdot Q_C^2 \tag{7}$$

where Q_C is the solar heat capturing capacity or transport load of the pipeline in units of MW_{th}. The average value for the friction factor is used as the constant value for estimating the pressure loss. For example, when the heat loads are 500–1000 MW_{th}, the average value of the friction factors is 0.0131, which yields an uncertainty of 8% for the range of 0.0122–0.0140. Then from the value of C_S, defined by equation

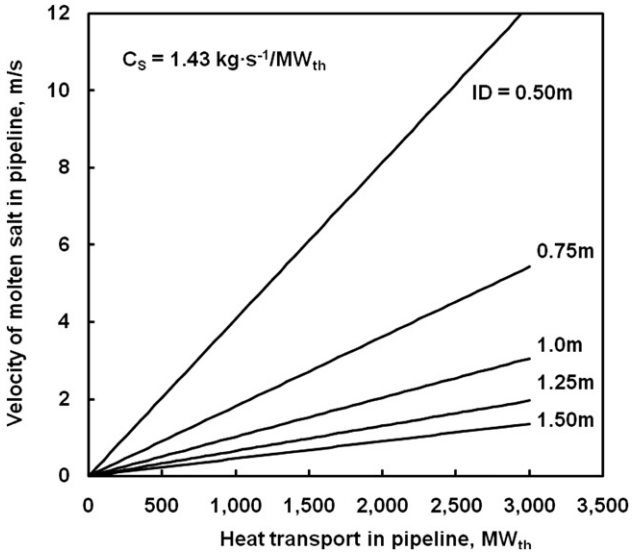

Fig. 5 – Influence of heat transport and pipeline diameter on the fluid velocity.

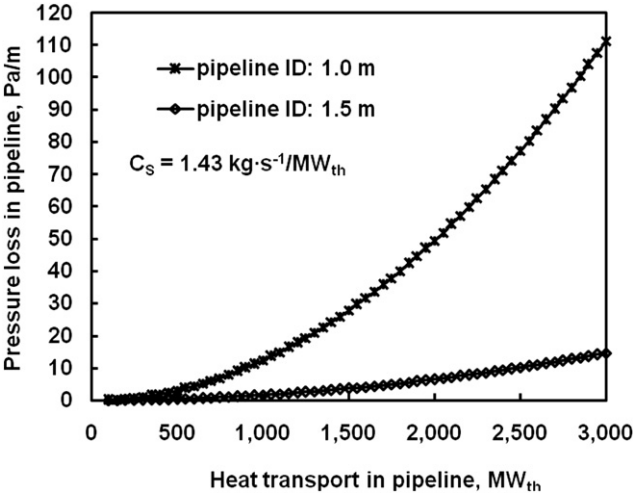

Fig. 6 – Relationship of pressure loss, heat load and pipeline diameter.

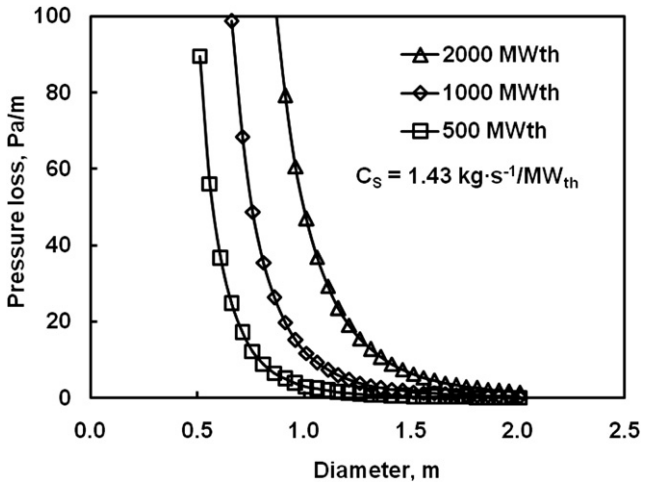

Fig. 7 – Influence of pipeline diameter on pressure loss.

(5), the pressure drop can be calculated with the simplified version of equation (7) as follows:

$$\frac{\Delta P}{L} = 1.237 \times 10^{-5} D_{pipe}^{-5} Q_C^2 \quad (8)$$

Figs. 6 and 7 show the dependence of pressure drop on heat load and pipeline diameter. For the pipeline diameter of 1.0 m, the pressure loss may reach 50 Pa/m or 0.5 bar/km when the heat transport load is 2000 MW$_{th}$ (about 400 t H_2/day). To pump the molten salt 10 km away, the pressure loss is 5 bars. This is a large pressure loss that may need additional pumps. To lower the pressure loss, the preferable measure is to increase the pipeline diameter since higher pressure can be avoided for a large diameter molten salt pipeline. Multiple pipelines can also decrease the pressure loss but may significantly increase the construction capital and maintenance costs. As shown in Fig. 6, at a transport load of 2000 MW$_{th}$, when the pipeline diameter increases by 50% from 1.0 to 1.5 m, the pressure loss decreases by 7.6 times from 49.5 to 6.5 Pa/m. The effect of diameters on the pressure drop Fig. 7 shows that 1.5 m is an optimum diameter for a pipeline that can deliver low pressure loss while meeting the required heat loads for various industrial hydrogen production scales from 100 to 400 t per day.

3.2. *Heat transport and heat loss in the transport pipeline*

When heat is transported to the hydrogen plant, it will experience some heat losses. As previously shown in Fig. 3, the temperature of solar salt in the storage tank is designed in the range of 675–700 °C, which is lower than the boiling point and 25–50 °C higher than 650 °C, so as to allow for heat loss from the pipeline and storage. It also meets the optimum heat distribution requirement of the Cu–Cl cycle after the molten salt reaches the hydrogen production plant. The parameters that influence the heat loss include the molten salt flow rate, heat load, temperature, pipeline diameter, pipeline flow characteristics, insulation, and weather conditions.

The heat loss is transferred from the molten salt to the pipe wall mostly through convection, and then through conduction of the insulation, and lastly through convection and radiation if the pipeline is on a ground surface. If the pipeline is buried underground, the heat loss will mostly flow to the soil. Since the thermal conductivity of metal is usually one order larger than most types of soils [45], the soil can also serve as insulation if the soil moisture is not significant.

Since the pipeline is long compared with its diameter, the axial flow effect will be neglected and the heat transfer can be approximated as a one-dimensional flow in the radial direction. The heat loss per unit length of the pipeline can be calculated with the following equation [47]:

Table 4 – Thermal properties of pipeline, molten salt, insulation and air for heat loss estimates.

Pipeline	Molten salt	Insulation			Air		
Thermal conductivity	Prandtl number	Thermal conductivity	Emissivity	T	Wind speed	Thermal conductivity	Prandtl number
15 W/m K Stainless steel AISI 304L [48,49]	0.895	0.25 W/m K Ceramic fiber blanket or ASTMC 177 high T Round Robin [49,50]	0.31 Heavily oxidized aluminum foil [51]	−50 °C	6.0 m/s Ontario, Canada [52]	0.0204 W/m K [53]	0.725 [53]

Table 5 – Heat transfer coefficients of the pipeline.

Pipe OD (wall thickness: 25.4 mm), m	Heat transport in pipeline,[a] MW$_{th}$	h_{convec}^{salt}, W/m^2 K	Insulation thickness θ, m	h_{convec}^{air}, W/m^2 K	h_{rad}, W/m^2 K
0.5	500	9946	0.25	19.7	1.48
	1000	18,816	0.50	18.3	1.48
1.0	500	2585	0.25	18.3	1.48
	1000	4700	0.50	17.4	1.48

a The mass flow rate of solar salt is calculated for heat transport in the pipeline with the solar heat capturing and storage capacity of $C_S = 1.4346$ kg s^{-1}/MW$_{th}$.

Table 6 – Contributions of various types of thermal resistances and heat transfer coefficients.

Contributions of various types of thermal resistances						
Pipe OD (wall thickness 25.4 mm), m	Convection of solar molten salt in pipeline		Insulation thickness θ, m	Conduction of pipe wall	Conduction of insulation	Convection and radiation to air
	$(1/R_i h^{salt}_{convec})$, m K/W	Heat transport load,[a] MW_{th}		$(\ln(R_0/R_i))/k_{pipe}$, m K/W	$(\ln[(R_0+\theta)/R_0])/k_{insu}$, m K/W	$1/((h^{air}_{convec}+h_{rad})(R_0+\theta))$, m K/W
0.5	0.0008	500	0.25	0.198	2.773	0.0942
0.5	0.0004	1000	0.50	0.198	4.394	0.0674
1.0	0.0004	500	0.25	0.100	1.622	0.0674
1.0	0.0002	1000	0.50	0.100	2.773	0.0529

a The mass flow rate of solar salt is calculated for this heat transport in the pipeline with the solar heat capturing and storage capacity of $C_S = 1.4346\ kg\,s^{-1}/MW_{th}$.

$$\frac{Q}{L}=\frac{2\pi(T_{salt}-T_{air})}{\frac{1}{R_i h^{salt}_{convec}}+\frac{\ln(R_0/R_i)}{k_{pipe}}+\frac{[\ln(R_0+\theta)/R_0]}{k_{insu}}+\frac{1}{\left(h^{air}_{convec}+h_{rad}\right)(R_0+\theta)}} \quad (9)$$

where Q/L is the heat loss per unit length, T_{salt} is the average salt temperature in the pipeline, T_{air} is the air temperature varying with days and seasons, R_i and R_o are the pipeline inside and outside diameters (not including the insulation), k_{pipe} is the thermal conductivity of the pipeline material, θ is the insulation thickness, h^{salt}_{convec} and h^{air}_{convec} are the convection heat transfer coefficients of salt flow in the pipeline and wind outside the insulation, and h_{rad} is the radiation heat transfer coefficient.

In equation (9), according to the ranges of Reynolds numbers and friction factors in the former sections, h^{salt}_{convec} can be calculated with the following equation [47],

$$Nu_{salt}=\frac{(f/8)Re_{salt}Pr_{salt}}{1+12.8(Pr^{0.68}_{salt}-1)\sqrt{f/8}} \quad (10)$$

where Nu_{salt} and Pr_{salt} are the Nusselt and Prandtl numbers calculated with the following equations:

$$Nu_{salt}=\frac{2R_{insu}\cdot h_{convection}}{k_{salt}} \quad (11)$$

$$Pr_{salt}=\frac{C^{salt}_P\cdot\mu_{salt}}{k_{salt}} \quad (12)$$

For the heat loss by wind outside the insulation, the convection heat transfer coefficient can be calculated based on the following equation [47]:

$$Nu_{wind}=0.3+\frac{0.62Re^{1/2}_{wind}Pr^{1/3}_{wind}}{\left[1+(0.4/Pr_{wind})^{2/3}\right]^{1/4}}\left[1+\left(\frac{Re_{wind}}{2.82\times10^5}\right)^{5/8}\right]^{4/5} \quad (13)$$

where Nu_{wind} and Pr_{wind} are the Nusselt and Prandtl numbers for wind.

For the heat loss by radiation, the heat transfer coefficient can be calculated with the following equation [47]:

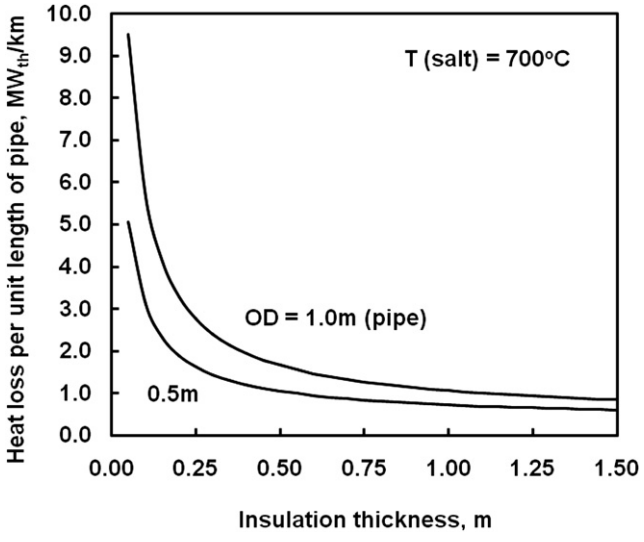

Fig. 8 – Influence of insulation thickness and temperature on heat loss in pipeline.

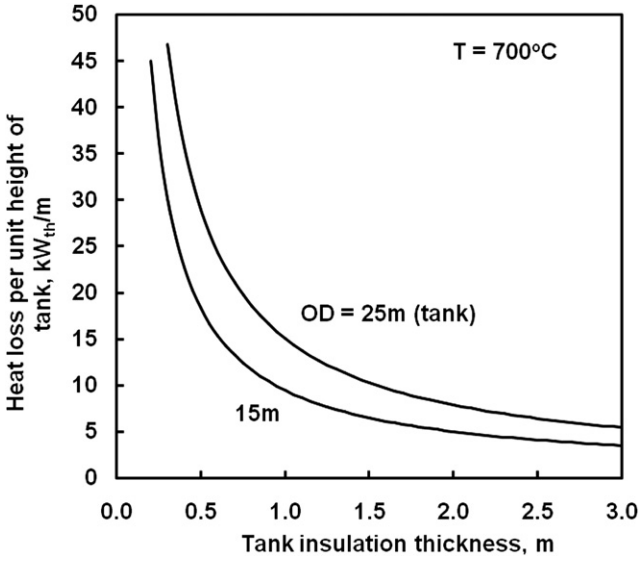

Fig. 9 – Influence of insulation thickness and temperature on heat loss of solar salt storage tank.

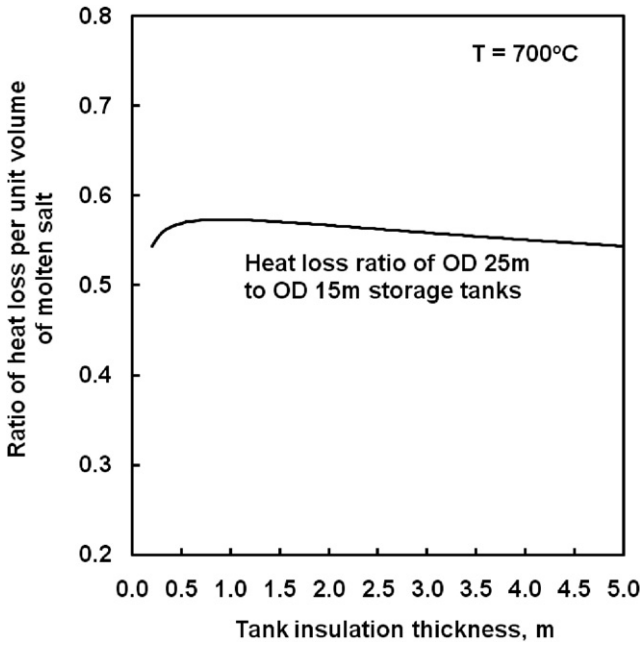

Fig. 10 – Influence of tank diameter on the heat loss of solar salt storage.

$$h_{rad} = \frac{\varepsilon \cdot \sigma \cdot \left(T_{insu}^4 - T_{air}^4\right)}{T_{insu} - T_{air}} \quad (14)$$

where σ is the Stefan–Boltzmann constant (5.6703×10^{-8} W/m^2 K^4), and ε is the emissivity coefficient of the insulation outer surface.

To have a safe design approximation, the upper value of the thermal conductivity of insulation for a very high temperature environment (800 °C) is adopted. It is also assumed that the outer surface of the insulation will be oxidized after some time so that the emissivity coefficient is higher than that of a well maintained condition. In addition, extreme cold weather conditions may occur occasionally. Table 4 shows the values used to calculate the heat loss.

Some calculated heat transfer coefficients and corresponding thermal resistance contributions are shown in Tables 5 and 6, respectively. Fig. 8 gives the heat losses based on the values in Tables 4–6. It can be found that the insulation can be designed to occupy more than 80% of the thermal resistance when the insulation thickness is larger than 0.25 m. The heat loss can be controlled to below 2MW$_{th}$/km when the insulation thickness is larger than 0.5 m. This shows the importance of the pipeline insulation. If considering both the pipeline diameter (e.g. 1.0 m) and insulation thickness (0.5 m), the total diameter will be at least 2.0 m, which may form a barrier for animals and human activities if the pipeline is constructed above ground. To bury the pipeline underground, this would increase construction and maintenance costs.

Assuming the cost of insulation is much lower than the pipeline, so that the insulation thickness can be constructed larger than 0.5 m, then the heat loss of 2.0 MW$_{th}$/km can be considered as a reasonable value for the transport. When the heat load is higher, the heat loss percentage is lower. If the pipeline is 10 km, then the heat loss is 20 MW$_{th}$. If the heat transport is 500 MW$_{th}$ (about 100 t H$_2$/day), the two-way heat loss is then about 12.5%. Fig. 8 also shows the challenge to reduce the heat loss: to increase the insulation thickness does not always have a significant heat loss reduction effect when the thickness is larger than 1.25 m.

The heat loss from the molten salt storage tank is also calculated with similar principles but a different one-dimensional assumption because the tank top and bottom also contribute a portion of heat losses. Fig. 9 shows the heat loss of molten salt storage tank per unit height. Assuming the cost of insulation is much lower than the tank, then the insulation thickness can be constructed larger than 2.0 m and the heat loss can be controlled lower than 10 kW$_{th}$/m. If the heat storage load is 500 MW$_{th}$ (about 100 t H$_2$/day), the heat loss is about 2%. One option to reduce the heat loss is to increase the tank diameter. Fig. 10 shows the heat loss difference for storing the same amount of molten salt with different tank diameters.

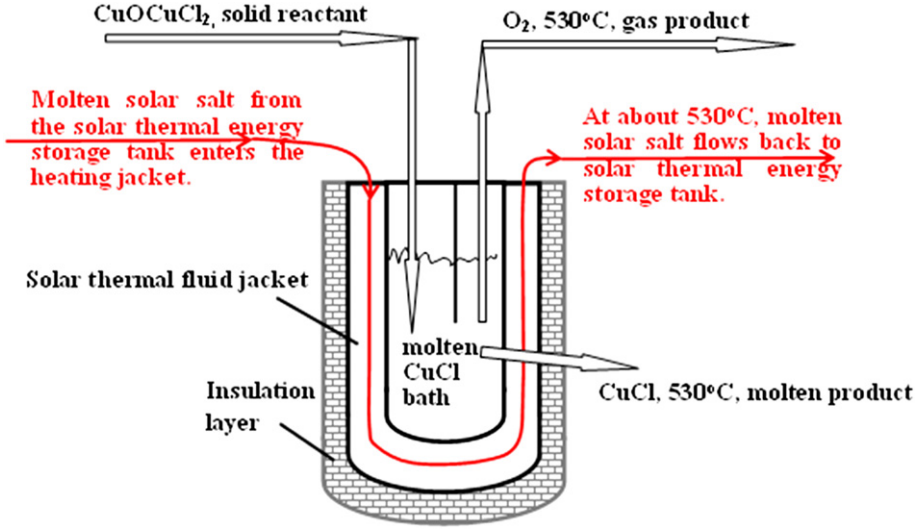

Fig. 11 – Solar thermal fluid flow through a heating jacket to supply heat to the molten CuCl produced in the oxygen reactor of the Cu–Cl cycle.

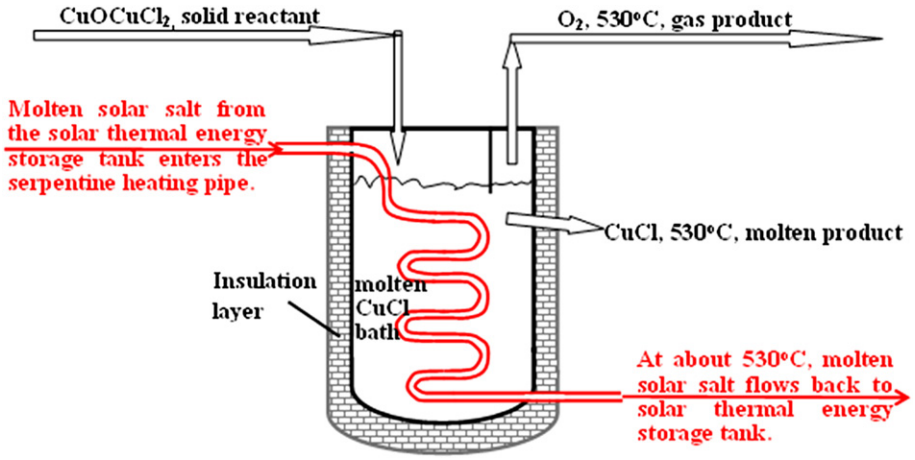

Fig. 12 – Solar thermal working fluid flow through a serpentine heating pipe to supply heat to the molten CuCl produced in the oxygen reactor of the Cu–Cl cycle.

Then the total heat loss of pipeline transport and storage is about 14.5%. Considering the heat loss through pumps and other components such as valves and expansion joints, the heat loss for a solar hydrogen plant design is assumed at about 20% when the transport distance is within 10 km. The analysis shown in Table 3 is based on this value.

4. Potential endothermic reactors for Cu–Cl cycle

As shown in equation (4), the oxygen production reaction that has the maximum temperature requirement is an endothermic reaction where molten CuCl is produced. This molten product brings significant advantages to the heat extraction from the solar thermal fluid that captures and stores the solar thermal energy. Conventional fluid–fluid heat exchangers can be used for the reactor design, in which the solar thermal fluid for capturing and storing solar heat can serve as the primary heat transport fluid in the pipeline. The molten CuCl product of the Cu–Cl cycle can work as the secondary fluid to extract heat from the primary fluid. The University of Ontario Institute of Technology (UOIT) is developing three types of oxygen production reactors that can be integrated with solar thermal working fluids, as shown in

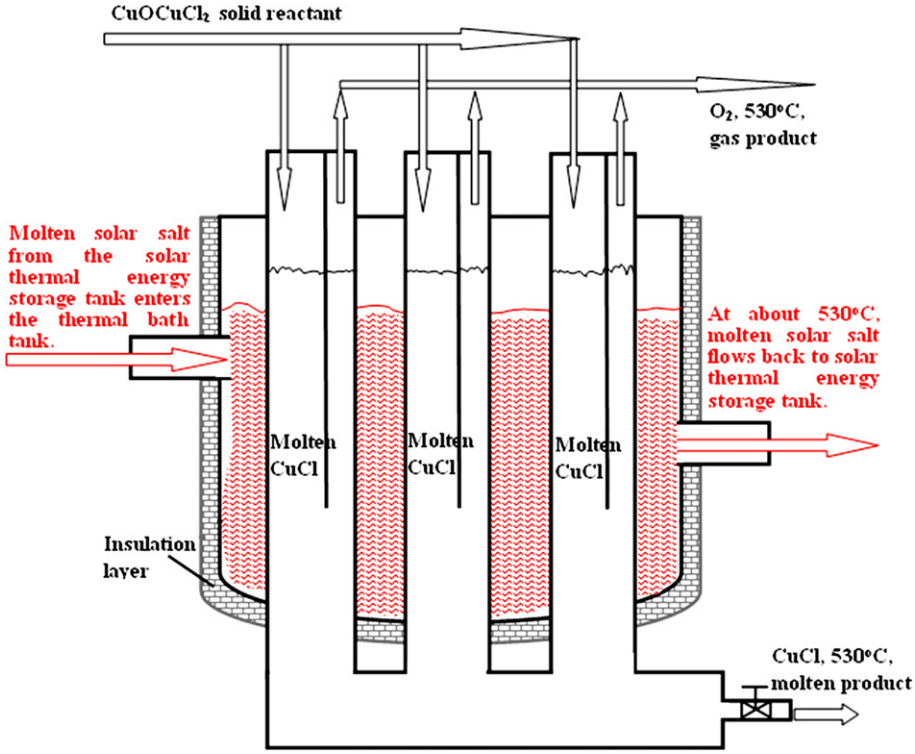

Fig. 13 – Solar thermal working fluid forms a thermal bath for a tubular oxygen reactor.

Figs. 11–13. Fig. 11 shows a reactor structure of a heating jacket type. The molten CuCl forms a thermal bath for solid reactant particles and heat is extracted from the high temperature solar thermal fluid flowing through the heating jacket. After the heat extraction, the solar working fluid can either be pumped back to the solar receiver atop the heliostat solar tower, or to the reactor of step 3 if the solar working fluid is steam. Fig. 12 shows a structure of built-in serpentine heating pipes, and Fig. 13 is a type of tubular reactor that is similar to a vertical shell and tube heat exchanger for a fast decomposition reaction. It can be concluded that due to the presence of molten product in the Cu–Cl cycle, the oxygen production reactor can also be a solar receiver without using another working fluid for the heat transfer.

5. Layout options for integration of the Cu–Cl cycle and heliostat solar tower

The temperature availability of the solar thermal working fluids in a current heliostat solar tower and the presence of molten CuCl product in the Cu–Cl cycle provide good flexibility for the integration. Fig. 14 shows the layout options for heat exchange between the Cu–Cl cycle and a heliostat solar thermal tower that uses molten salt. The flowchart is based on current operational and planned technology where the molten salt in the solar receiver gives an outlet temperature of 650–700 °C that can supply the Cu–Cl cycle. The temperatures of water streams in the layout were calculated according to the water stream enthalpy change and expansion ratios that were reported previously [40,41]. The water stream circulation illustrated in Fig. 14 has the typical features of a single-reheat system that uses a preheater and two types of turbines, i.e., high pressure (HP) turbine and low pressure (LP) turbine.

It can be found that point L, i.e., the location immediately downstream of the solar receiver, has the maximum temperature that can supply heat for step 4 of the Cu–Cl cycle, which requires 530 °C. Therefore, at this location, a bypass line of the solar molten salt (primary fluid) passing points L, J, and D can be designed for heat extraction from a solar tower to the Cu–Cl hydrogen production cycle.

For step 3 of the Cu–Cl cycle, the temperature requirement is 375 °C. The heat for this step can be supplied by several sources: 1) solar thermal salt at a temperature of 530 °C exiting step 4, i.e., the route passing point E; 2) the solar thermal salt at temperatures of 650–700 °C flowing out of the heat exchanger, i.e., the route passing through points L, J and K; 3) the steam exiting the steam generator, i.e., the route passing through

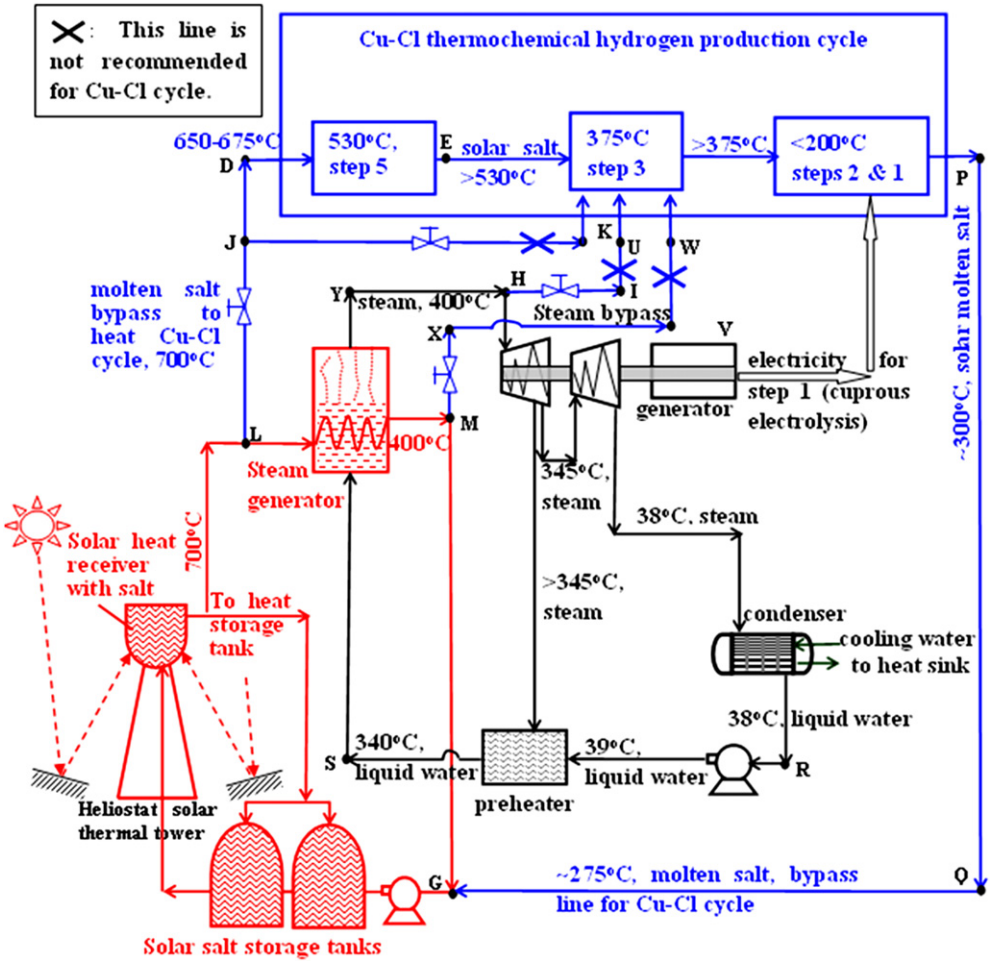

Fig. 14 – Integration of a heliostat Cu–Cl thermochemical hydrogen production cycle and a heliostat solar thermal power plant that uses molten salt as the working fluid.

points Y, H, I and U; and 4) the solar thermal fluid at temperatures of around 400 °C exiting the steam generator, i.e., the route passing through points M, V and W.

The first option appears most preferable since this arrangement can meet the optimum heat distribution structure of the Cu–Cl cycle and also reduce the number of bypass lines so that the complexity of the layout can be reduced. However, if the heat carried by the solar fluid exiting step 4 cannot supply sufficient energy for step 3, then the second option is most preferable, but at the cost of lowering the thermal efficiency of hydrogen production. The advantage of the third option is to directly supply water for the hydrogen production, but the heat carried by the steam may not be sufficient to support step 3. Option 4 is not recommended because the solar thermal fluid at 400 °C carries much less heat than 530 °C in option 1. Moreover, option 4 means the construction of more bypass lines for the solar thermal fluid. More bypass lines may also result in unpredictable safety issues, since the loop is more open to corrosive chemicals of the Cu–Cl cycle.

6. Conclusions

From the perspective of the compatibility with thermochemical hydrogen production cycles, this paper examined the temperatures of various solar thermal energy technologies, including currently operational, under construction and to be announced. It is found that a heliostat solar thermal tower can provide the required high temperature thermal energy for hydrogen production. Due to a lower temperature requirement than other thermochemical hydrogen production cycles, the Cu–Cl cycle is a promising option for integration with current operational heliostat solar towers. The heat requirements are also examined and it is found that the solar heat source must be sufficiently high and above the maximum temperature requirement of the hydrogen production cycle, in order to match the optimum heat requirements. The quantity of solar molten salt and solar plant dimensions for capturing and storing solar heat for an industrial hydrogen production scale are also examined. It is concluded that there are two major challenges of solar thermal plants for 24-h-use per day, namely large land area and molten salt quantity.

The flow characteristics and heat losses of the heat transport pipelines are also studied and it is found that the pipeline diameter has the most significant effect on the pressure drop. The optimum pipeline diameter is about 1.5 m in order to achieve a reasonable flow velocity and reduced pressure loss. The heat loss from the pipeline is mainly reduced by the insulation, among other influencing factors such as heat load and weather conditions.

The heat loss from the solar salt storage tank is also calculated and it shows that the heat loss from the storage tank is much lower than that by the transport pipeline. Increasing the storage tank diameter can significantly decrease the heat losses. The total heat loss through the transport pipeline and storage tank can be designed below 20% for industrial hydrogen productions scales of 100–400 t per day if the transport distance is within 10 km.

The molten CuCl produced in the oxygen production step of the Cu–Cl cycle allows efficient heat transfer and use of currently available heat exchangers for linkage of a Cu–Cl cycle with current solar thermal molten salts for capturing and storing the solar radiation. It will also allow other solar working fluids such as steam and gases. This paper investigates several types of heat exchangers for the linkage and layout options. The layout options are given for linkage of the Cu–Cl cycle with a heliostat solar thermal tower in this paper.

Acknowledgements

Financial support of this research from the Ontario Research Fund and the Province of Ontario is gratefully acknowledged.

REFERENCES

[1] NYSERDA (New York State Energy Research and Development Authority). Hydrogen Fact Sheet: Hydrogen production – steam methane reforming (SMR). Technical Report – Clean Energy Initiative. Available from: http://www.getenergysmart.org/files/hydrogeneducation/6hydrogenproductionsteammethanereforming.pdf [accessed 1.05.10].
[2] Lewis MA, Masin JG. The evaluation of alternative thermochemical cycles – part II: the down-selection process. International Journal of Hydrogen Energy. 2009;34:4125–35.
[3] Wilhelm E, Fowler M. A technical and economic review of solar hydrogen production technologies. Bulletin of Science, Technology and Society. 2006;26:278–87.
[4] Schultz K. Thermochemical production of hydrogen from solar and nuclear energy. Technical Report of General Atomics; 2003. Available from: http://gcep.stanford.edu/pdfs/hydrogen_workshop/Schultz.pdf [accessed 20.04.10].
[5] Steinfeld A. Solar thermochemical production of hydrogen – a review. Solar Energy 2005;78:603–15.
[6] Wang ZL, Naterer GF, Gabriel KS, Gravelsins R, Daggupati VN. Comparison of sulfur–iodine and copper–chlorine thermochemical hydrogen production cycles. International Journal of Hydrogen Energy 2009;35:4820–30.
[7] Makhijani A. Nuclear power and CO_2 emission reductions comments on radioactive waste management and relative costs of options. IEER (Institute of Energy and Environmental Research) Report; 2009. Available from: http://www.ieer.org/carbonfree/NuclearPower_wastes_and_CO2_cost_reduction_considerations.pdf [accessed 20.04.10].
[8] Pearce JM. Thermodynamic limitations to nuclear energy deployment as a greenhouse gas mitigation technology. International Journal of Nuclear Governance, Economy and Ecology 2008;2:113–30.
[9] Bodansky D. The environmental paradox of nuclear power. Environmental Practice 2001;3:86–8.
[10] Perkins C, Weimer AW. Likely near-term solar-thermal water splitting technologies. International Journal of Hydrogen Energy 2004;29:1587–99.
[11] Weimer, A. Development of solar-powered thermochemical production of hydrogen from water. DOE (Department of Energy, US) Report; 2005. Available from: http://www.hydrogen.energy.gov/pdfs/review05/pd28_weimer.pdf [accessed 10.04.10].
[12] Srinivasan NK, Michael JV. The thermal decomposition of water. International Journal of Chemical Kinetics 2006;38:211–9.
[13] Wang ZL, Naterer GF, Gabriel KS, Gravelsins R, Daggupati VN. Comparison of different copper–chlorine thermochemical cycles for hydrogen production. International Journal of Hydrogen Energy 2009;34:3267–76.

[14] UNEP (United Nations Environment Programme) Division of Technology, Industry and Economics. Energy technology fact sheet: solar thermal. Technical Report of Global Solar Thermal Energy Council; 2002. Available from: http://www.solarthermalworld.org/files/Solar%20Thermal%20Fact%20Sheet.pdf?download [accessed 10.04.10].
[15] eSolar. Sierra suntower – a new blueprint for solar energy. Technical Report. Available from: http://www.esolar.com/sierra_fact_sheet.pdf [accessed 10.04.10].
[16] NREL (National Renewable Energy Lab). Concentrating solar power projects – Sierra SunTower. Technical Report. Available from: http://www.nrel.gov/csp/solarpaces/project_detail.cfm/projectID=63 [accessed 20.04.10].
[17] NREL (National Renewable Energy Lab). Concentrating solar Power: energy from mirrors. Technical Report DOE/GO-102001-1147; 2001. Available from: http://www.nrel.gov/docs/fy01osti/28751.pdf [accessed 20.04.10].
[18] Concentrated solar thermal power. New Energy direction – exploring alternative energy technology. Available from: http://newenergydirection.com/blog/2008/12/concentrated-solar-thermal-power/ [accessed 7.05.10].
[19] Solúcar. 10 MW Solar Thermal Power Plant for Southern Spain. Final Technical Progress Report; 2006. Available from: http://ec.europa.eu/energy/res/sectors/doc/csp/ps10_final_report.pdf [accessed 7.05.10].
[20] Solar Tower, Seville, Spain. Available from: http://www.power-technology.com/projects/Seville-Solar-Tower/ [accessed 20.05.10].
[21] Taggart S. Hot stuff: CSP and the power tower. Renewable Energy Focus:51–4. Available from: http://www.trec-uk.org.uk/articles/REF/ref_0903_pg51_55.pdf; 2008 [accessed 7.05.10].
[22] European Commission. Solar hybrid gas turbine electric power system. Solgate Progress Report. EUR 21615. Available from: http://ec.europa.eu/research/energy/pdf/solgate_en.pdf [accessed 7.05.10].
[23] Schmitz M. Salt-free solar: CSP tower using air. Renewable Energy World Magazine. Available from: http://www.renewableenergyworld.com/rea/news/article/2009/03/salt-free-solar-csp-tower-using-air; 2009 [accessed 20.05.10].
[24] Developments in solar power towers. Available from: http://ecofuture.net/aliceinwonderland/solar-power-towers/51/ [accessed 20.05.10].
[25] SolarPACES. Solar power tower. Technical report. pp. 5-6–5-23. Available from: http://www.solarpaces.org/CSP_Technology/docs/solar_tower.pdf [accessed 20.05.10].
[26] S. Patel. Interest in solar tower technology rising. In: Electric power conference & exhibition; 2009. Available from: http://www.powermag.com/renewables/solar/Interest-in-Solar-Tower-Technology-Rising_1876.html [accessed 20.05.10].
[27] Martín JC. Solar Tres – first commercial molten salt central receiver. In: NREL CSP technology workshop. Denver, US. March 7; 2007.
[28] BrightsourceEnergy. Technology overview. Available from: http://www.jspsusa-sf.org/junba/docs/junba2009/techfair/A-1-3BrighSourceEnergy.pdf; 2009 [accessed 20.05.10].
[29] Way J. Storing the sun: molten salt provides highly efficient thermal storage. Available from: http://www.renewableenergyworld.com/rea/news/article/2008/06/storing-the-sun-molten-salt-provides-highly-efficient-thermal-storage-52873; 2008 [accessed 27.05.10].
[30] Wang Z, Yao Z, Dong J, Jin H, Han W, Lu Z, et al. The design of a 1 MW solar thermal tower plant in Beijing, China. In: Proceedings of ISES World Congress 2007 (Vol. I–Vol. V) – solar energy and human settlement. Beijing, China; 2007. September 18–21, 2007.
[31] T-Raissi A, Huang C, Muradov N. Hydrogen production via solar thermochemical water splitting; 2007. Technical report of NASA (National Aeronautics and Space Administration). NASA/CR—2009-215441. p. 23–196.
[32] Beghi B. A decade of research on thermochemical water hydrogen at the joint research center, Ispra. International Journal of Hydrogen Energy 1986;11:761–71.
[33] Lewis MA, Taylor A. High temperature thermochemical processes. DOE Hydrogen Program. Annual Progress Report, Washington DC; 2006. 182–185.
[34] Sakurai M, Nakajima H, Amir R, Onuki K, Shimizu S. Experimental study on side-reaction occurrence condition in the iodine–sulfur thermochemical hydrogen production process. International Journal of Hydrogen Energy. 2000;23:613–9.
[35] Kubo S, Kasahara S, Okuda H, Terada A, Tanaka N, Inaba Y, et al. A pilot test plan of the thermochemical water-splitting iodine–sulfur process. Nuclear Engineering and Design 2004;233:355–62.
[36] Abanades S, Charvin P, Flamant G, Neveu P. Screening of water-splitting thermochemical cycles potentially attractive for hydrogen production by concentrated solar energy. Energy 2006;31:2805–22.
[37] Brown LC, Besenbruch GE, Schultz KR, Marshall AC, Showalter SK, Pickard PS, et al. Nuclear production of hydrogen using thermochemical water-splitting cycles. Technical report of GA (General Atomics, US). GA-A23944. Available from: https://fusion.gat.com/pubs-ext/MISCONF02/A23944.pdf; 2002 [accessed 22.05.10].
[38] Tamaura Y, Steinfeld A, Kuhn P, Ehrensberger K. Production of solar hydrogen by a novel, 2-step, water splitting thermochemical cycle. Energy 1995;20:325–30.
[39] NREL (National Renewable Energy Lab). Assessment of thermal energy storage for parabolic trough solar power plants. Available from: http://www.nrel.gov/csp/troughnet/pdfs/kearney_tes_overview.pdf [accessed 27.05.10].
[40] Naidin M, Mokry S, Baig F, Gospodinov Y. Thermal-design options for pressure-channel SCWRS with cogeneration of hydrogen. Journal of Engineering for Gas Turbines and Power 2009;V131:012901-1–012901-8.
[41] Buongiorno J, Swindeman R, Corwin W, Rowcliffe A, MacDonald P, Was G, et al. Supercritical water reactor (SCWR) survey of materials experience and R&D needs to assess viability. Technical report Prepared for the U.S. Department of Energy Assistant Secretary Under DOE Idaho Operations Office Contract DE-AC07-99ID13727. Idaho National Engineering and Environmental Laboratory, Bechtel BWXT Idaho, LLC; September 2003.
[42] American Nuclear Society, Nuclear power: a sustainable source of energy. Technical Report. Available from: http://www.ans.org/pi/resources/brochures/docs/power.pdf [accessed 21.05.10].
[43] Reilly HE. "Solar power tower". SNL R&D Award Entry Form; 2000. Available from: http://www.azsolarcenter.org/images/articles/tech-science/solar-power-tower.pdf [accessed 6.06.10].
[44] Laurent Steven St .. Thermocline thermal storage test for large-scale solar thermal power plants, Sept 9, 2000. Report number: DE00-761869 AND2000-2059C. DOE Scientific and Technical Information. Available from: http://www.osti.gov/bridge/purl.cover.jsp;jsessionid=2AFF77CA5ABCBC4D8726F129A505A76C?purl=/761869-hh1dP8/webviewable/ [accessed 22.05.10].
[45] Soil thermal conductivity. Available from: http://www.geo4va.vt.edu/A1/A1.htm [accessed 15.11.10].
[46] Forsberg CW. Hydrogen, nuclear energy, and the advanced high-temperature reactor. International Journal of Hydrogen Energy 2003;28:1073–81.
[47] Lienhard IV JH, Lienhard V JH. A heat transfer textbook. 3rd ed.... Cambridge, Massachusetts, USA: Phlogiston Press; 2008. p. 341–594 [chapters III and IV].

[48] Assael MJ, Gialou K. Measurement of the thermal conductivity of stainless steel AISI 304L up to 550 K. International Journal of Thermophysics July 2003;24:1145–53.
[49] Desjarlais AO, Zarr RR. Insulation materials, vol. 4; 2002;, ISBN 0-8031-2898-3; 2002. Bridgeport, NJ, US. p. 122–8.
[50] Microtherm technical data. Available from: http://www.microthermgroup.com/EXEN/site/eng_thermcondgraph.aspx [accessed 2.11.10].
[51] The radiation heat transfer emissivity coefficient of some common materials as aluminum, brass, glass and many more. Available from: http://www.engineeringtoolbox.com/emissivity-coefficients-d_447.html [accessed 4.10.10].
[52] Ontario government data. Available from: http://www.omafra.gov.on.ca/english/engineer/facts/03-047.htm#f13 [accessed 4.10.10].
[53] Temperature, density, specific heat, thermal conductivity, expansion coefficient, kinematic viscosity and Prandtl's number for temperatures ranging −150 to 400 °C. Available from: http://www.engineeringtoolbox.com/air-properties-d_156.html [accessed 4.10.10].